Zoological Studies **61**:86 (2022)
doi:10.6620/ZS.2022.61-86

Zoological Studies

Open Access

Macrobiotus hupingensis, a New Tardigrade Species in the *Macrobiotus pallarii* Complex from China

Zhimin Yuan[1,*], Yan Wang[1], Qiuju Liu[1], Lijie Liu[1], and Xiaochen Li[1]

[1]*College of Life Sciences, Shaanxi Normal University, Xi'an, 710100, P. R. China. *Correspondence: E-mail: yuanzhimin@snnu.edu.cn (Yuan). E-mail: 1957511977@qq.com (Wang); liuqj1126@126.com (Liu); liulijie0803@163.com (Liu); xiaochen@snnu.edu.cn (Li)*

Received 3 March 2021 / Accepted 17 October 2022 / Published 26 December 2022
Communicated by Benny K.K. Chan

In this paper we describe *Macrobiotus hupingensis*, a new tardigrade species of the *Macrobiotus pallarii* complex from southern China. We used the traditional morphology-based taxonomic analysis, supported by detailed morphometrics, light microscopy imaging, scanning electron microscopy, and analysis of four genetic markers (18S rRNA, 28S rRNA, *COI* and ITS-2). *Macrobiotus hupingensis* sp. nov. is characterized by eggs with large, conical processes, each surrounded by six (only sometimes five) hexagonal areolae. Based on the morphological characters of the animals (two macroplacoids, one microplacoid, porous curicle, Y-shaped claws) as well as genetic data, we demonstrate the new species to be a member of the *M. pallarii* complex. However, it differs specifically from *M. pallarii*, *M. pseudopallarii*, and *M. ripperi* mainly by the absence of sparse granulation between legs III and IV. It also differs from *M. margoae* mostly by the presence of meshes within the entire egg process wall. Finally, the new species can be easily distinguished from *M. caymanensis* by the presence of granulation visible in light microscopy in all legs.

Key words: China, DNA barcoding, *Macrobiotus hupingensis* sp. nov., Species delimitation.

BACKGROUND

Before this study, 234 tardigrade species had been recorded in China (Gao et al. 2012; Sun 2014; Yang 2015; Zawierucha et al. 2018; Bi 2019; Sun et al. 2020; Guo 2020) and more than 1,300 had been found and described worldwide (Guidetti and Bertolani 2005; Degma and Guidetti 2007; Degma et al. 2009–2021).

The genus *Macrobiotus* C.A.S. Schultze, 1834, is the most speciose and diverse in the family Macrobiotidae and was the first described tardigrade genus (Greven 2018). The genus currently comprises 119 species and 2 subspecies (Stec et al. 2020a b 2021a b 2022; Degma et al. 2009–2021; Vecchi et al. 2022; Cesari et al. 2022) (Table S1), 27 of which are doubtful because of insufficient descriptions (they often lack information on key traits that are currently used to differentiate the species, such as leg granulation, lunule morphology, oral cavity armature, morphometric characters, and egg ornamentation). At present, 27 species of the genus *Macrobiotus* have been recorded in China (Table 1) (Gao et al. 2012; Sun 2014; Yang 2015; Bi 2019; Guo 2020; Wang 2021). *Macrobiotus* is characterised by porous cuticle, mouth opening surrounded by ten peribuccal lamellae, a rigid buccal tube strengthened with the ventral lamina lacking a ventral hook, two macroplacoids and one microplacoid in the pharynx, double Y-shaped claws on each leg and by laying ornamented eggs freely in the environment. Animals in the *Macrobiotus pallarii* complex have the very typical morphology of *Macrobiotus*. However, this group is characterized by egg ornamentation composed of large conical processes separated by a single row of areolation (such ornamented eggs are also known in

Citation: Yuan Z, Wang Y, Liu Q, Liu L, Li X. 2022. *Macrobiotus hupingensis*, a new tardigrade species in the *Macrobiotus pallarii* complex from China. Zool Stud **61**:86. doi:10.6620/ZS.2022.61-86

other genera, *e.g.*, *Paramacrobiotus* Guidetti et al. 2009 or *Mesobiotus* Vecchi et al. 2016).

The Wuling Mountains are in southern Central China. The entire area is covered by folded mountains, with elevations generally above 1000 m asl, an average temperature of about 13.4°C, and average precipitation reaching 1100–1600 millimetres. The district has a transitional climate from subtropical to warm temperate zones, forest coverage rate is as high as 53%, and the vegetation is mixed broadleaf evergreen and deciduous forest (Liu et al. 2020). The mountains run from northeast to southwest and stretch across Chongqing, Hunan, Hubei, and Guizhou Provinces (Chen and Li 2003). Until now, no tardigrade fauna was reported from Wuling Mountains. However, in the summer of 2019, we made a field trip to the Wuling Mountains and identified a new species from the genus *Macrobiotus*, which we describe here. Our research applied an integrative approach to taxonomy involving detailed morphological, morphometric, and molecular analyses. Such an integrated approach let us accurately test a new species hypothesis.

MATERIALS AND METHODS

Sample and specimens

Moss was collected from the surface of a rock located at Hupingshan, Wuling Mountains, Hunan Province, China (29°50'–30°09'N, 110°29'–110°59'E; 1000–2000 m asl) in August 2019. Samples were examined for tardigrades using the protocol by Dastych (1980) with modifications described in detail in Stec et al. (2015). A total of 236 individuals and 46 eggs of the new species were extracted from the sample and split into three groups: morphological analysis with phase and differential contrast light microscopy (PCM), morphological analysis with scanning electron microscopy (SEM), and DNA sequencing.

Microscopy and imaging

Specimens were fixed on permanent microscope slides in Hoyer's medium for observations and morphometry using phase contrast light microscopy (PCM). Images were captured with a Nikon DS-Fil

Table 1. A list of species of *Macrobiotus* formally described from China before (valid and doubtful taxa)

State	Species formally recorded in China	References
valid	*Macrobiotus alvaroi* Pilato & Kaczmarek, 2007	Guo 2020
	Macrobiotus ariekammensis Węglarska, 1965 [*Macrobiotus adelges* Dastych, 1977]	Gao et al. 2012
	Macrobiotus crenulatus Richters, 1904 [*Macrobiotus dentatus* Binda, 1974]	Sun 2014
	Macrobiotus diversus Biserov, 1990	Sun 2014
	Macrobiotus drakensbergi Dastych, 1993	Guo 2020
	Macrobiotus echinogenitus Richters, 1903	Gao et al. 2012
	Macrobiotus hufelandi C.A.S. Schultze, 1834 [*Macrobiotus schultzei* Greeff, 1866 according to Marcus 1928]	Gao et al. 2012
	Macrobiotus mandalaae Pilato, 1974	Gao et al. 2012
	Macrobiotus nelsonae Guidetti, 1998	Guo 2020
	Macrobiotus occidentalis occidentalis Murray, 1910	Gao et al. 2012
	Macrobiotus pallarii Maucci, 1954 [*Macrobiotus aviglianae* Robotti, 1970]	Sun 2014
	Macrobiotus patagonicus Maucci, 1988	Bi 2019
	Macrobiotus paulinae Stec, Smolak, Kaczmarek & Michalczyk, 2015	Guo 2020
	Macrobiotus persimilis Binda & Pilato, 1972	Gao et al. 2012
	Macrobiotus polyopus Marcus, 1928	Guo 2020
	Macrobiotus ragonesei Binda, Pilato, Moncada & Napolitano, 2001	Gao et al. 2012
	Macrobiotus ramoli Dastych, 2005	Guo 2020
	Macrobiotus recens Cuénot, 1932	Gao et al. 2012
	Macrobiotus shonaicus Stec, Arakawa & Michalczyk, 2018	Guo 2020; Wang 2021
doubtful	*Macrobiotus annae* Richters, 1908	Sun 2014
	Macrobiotus gemmatus Bartoš, 1963	Gao et al. 2012
	Macrobiotus hibiscus de Barros, 1942	Gao et al. 2012
	Macrobiotus insignis Bartoš, 1963	Gao et al. 2012
	Macrobiotus rollei Heinis, 1920	Gao et al. 2012
	Macrobiotus shennongensis Yang, 1999	Yang 2015
	Macrobiotus terricola Mihelčič, 1951	Gao et al. 2012
	Macrobiotus yunshanensis Yang, 2002	Yang 2015

digital camera, and measurements were made using the embedded software. Immediately after mounting the specimens in the medium, slides where checked under PCM for the presence of males and females in the studied population based on the spermatozoa in testis and spermathecae, which remain visible for several hours after mounting (Coughlan et al. 2019; Coughlan and Stec 2019). To obtain clean and extended specimens for SEM, tardigrades were processed according to the protocol by Stec et al. (2015). Specimens were examined under a low-vacuum environmental scanning electron microscopy—SEM (Tabletop Microscope TM3030 Plus, Hitachi, Tokyo, Japan)—at Shaanxi Normal University, Xian, China. All figures were assembled in Photoshop CS6.

Morphometrics and morphological nomenclature

All measurements are given in micrometres (µm). Structures were measured only if they were in the proper orientation. Structures were measured only if their orientation was suitable. Body length was measured from the anterior extremity to the end of the body, excluding the hind legs. The terminology used to describe oral cavity armature and eggshell morphology follows Michalczyk and Kaczmarek (2003) and Kaczmarek and Michalczyk (2017). The terminology used to describe cuticular bars and muscle attachments on legs follows Kiosya et al. (2021). Macroplacoid length was measured according to Kaczmarek et al. (2014). Buccal tube length and the level of the stylet support insertion point were measured according to Pilato (1981). The *pt* index is the ratio of the length of a given structure to the length of the buccal tube expressed as a ratio (Pilato 1981). Measurements of buccal tube widths and heights of claws and eggs follow Kaczmarek and Michalczyk (2017). Morphometric data were analysed with the Parachela ver. 1.7 template available from the Tardigrada Register, http://www.tardigrada.net/register (Michalczyk and Kaczmarek 2013), and are provided in the Supplementary Materials (Table S2). Tardigrade taxonomy follows Bertolani et al. (2014), Stec et al. (2020c 2021c).

Genotyping

The DNA was extracted from individual animals with the TIANamp Micro DNA Kit (Tiangen) following the manufacturer's standard protocols. We sequenced four DNA fragments: the small ribosomal subunit (18S rRNA, nDNA), large ribosomal subunit (28S rRNA, nDNA), internal transcribed spacer (ITS-2, nDNA), and cytochrome oxidase subunit I (*COI*, mtDNA). All fragments were amplified and sequenced according to the protocols described in Stec et al. (2020b); primers and original references for specific PCR programs are listed in table 2.

Sequencing products were read with the ABI 3130xl sequencer at Tsingke Biology Limited Company, Xian, China. Sequences were processed in BioEdit ver. 7.2.5 (Hall 1999) and submitted to GenBank. See table 3 for accession numbers.

Phylogenetic analysis and *p*-distances

The phylogenetic analyses were conducted using *COI* sequences. Sequences were downloaded from GenBank or produced *de novo* (Table 3). Type sequences of *Macrobiotus caelestis* (Coughlan et al. 2019) were used as the outgroup. The sequences were aligned using MAFFT ver. 7 (Katoh et al. 2002; Katoh and Toh 2008). The *COI* sequences were aligned according to their amino acid sequences (translated using the invertebrate mitochondrial code) with the MUSCLE algorithm (Edgar 2004) in MEGA X version 10.1.7 (Kumar et al. 2018) with default settings (*i.e.*, all gap penalties = 0, max iterations = 8, clustering method = UPGMB, lambda = 24). Alignments were visually inspected and trimmed in MEGA X. Sequences

Table 2. Primers and references for PCR protocols for amplification of the four DNA fragments sequenced in this study

DNA fragment	Primer name	Primer direction	Primer sequence (5'-3')	Primer source	PCR program
18S rRNA	SSU01_F	forward	AACCTGGTTGATCCTGCCAGT	Sands et al. (2008)	Zeller (2010)
	SSU82_R	reverse	TGATCCTTCTGCAGGTTCACCTAC		
28S rRNA	28S_Eutar_F	forward	ACCCGCTGAACTTAAGCATAT	Gąsiorek et al. (2018)	Mironov et al. (2012)
	28SR0990	reverse	CCTTGGTCCGTGTTTCAAGAC	Mironov et al. (2012)	
ITS-2	Eutar_Ff	forward	CGTAACGTGAATTGCAGGAC	Stec et al. (2018)	Wełnicz et al. (2011)
	Eutar_Rr	reverse	TCCTCCGCTTATTGATATGC		
COI	LCO1490	forward	GGTCAACAAATCATAAAGATATTGG	Folmer et al. (1994)	Michalczyk et al. (2012)
	HCO2198	reverse	GTAAATATATGRTGDGCTC		

were concatenated with PhyloSuite v1.2.2 (Zhang et al. 2020). Model selection and phylogenetic reconstructions were undertaken using the CIPRES Science Gateway (Miller et al. 2010). Model selection was performed for each alignment partition using PartitionFinder2 (Lanfear et al. 2016). Maximum Likelihood (ML) phylogenetic reconstruction was performed using MEGA X. Bootstrapping was done with 500 replicates for ML trees. The phylogenetic tree was visualised using iTOL v6.5.2 (https://itol.embl.de/), and the image was edited with Photoshop CS6.

The species in the *M. pallarii* complex are phylogenetically and morphologically distinct (Stec et al. 2021a), so the *p*-distances for the genetic differential diagnosis were calculated between species in the *M. pallarii* complex for the four sequenced markers separately (18S rRNA, 28S rRNA, ITS2, and *COI*) using the alignments used for analysis. Pairwise distances were calculated with the software MEGA X using pairwise deletion for the Gap/Missing Data Treatment option. Detailed *p*-distance tables are provided in table S3.

Species delimitation

To assess the genetic differentiation of species within our dataset of 18 *Macrobiotus pallarii* complex *COI* sequences, we used the ASAP procedure designated for a list of partitions of species hypotheses using genetic distances, calculated between DNA sequences, and ranked the partitions by their ASAP-scores: the lower the score, the better the partition (Puillandre et al. 2021). The online ASAP version (https://bioinfo.mnhn.fr/abi/public/asap/asapweb.html) was used with default settings and the K2P distance model.

Statistical analysis

Statistical analyses were run in SPSS software (version 23.0; SPSS Inc., Chicago, IL, USA). Morphometric data for eggs and animals were analysed with principal component analysis (PCA). We analysed the eggs and animals using absolute values (raw measurements in µm) and relative (*pt*) values, respectively. Missing data in the animal dataset were replaced with median site data in SPSS. PCA extracts maximum variance from a dataset with a few orthogonal components. The first principal component (PC1) is the linear combination of observed variables that maximally separates the subjects by maximizing the variance of their component scores. The second component (PC2) is the linear combination of the observed variables

Table 3. GenBank accession numbers of sequences used in the present study. Newly generated sequences are in bold

Taxon	Individual	18S	28S	*COI*	ITS2
Macrobiotus caelestis		MK737073	MK737071	MK737922	MK737072
Macrobiotus pallarii complex	hp04130206	**MW183923**		**MZ474842**	
	hp04130207		**MZ470349**	**MZ474843**	
	hp04130208		**MZ470350**		**MW186952**
	hp04130209				**MW187003**
	FI.066.1	MT809075	MT809088	MT807929	
	FI.066.2	MT809076	MT809089	MT807930	MT809103
	FI.066.3			MT807931	MT809104
	FI.066.4			MT807932	MT809105
	IT.337.1	MT809069	MT809081	MT807924	MT809094
	IT.337.2	MT809070	MT809082	MT807925	MT809095
	IT.337.3	MT809071	MT809083	MT807926	MT809096
	ME.007.1	MT809065	MT809077		MT809090
	ME.007.2	MT809066	MT809078	MT807920	
	ME.007.3	MT809067	MT809079	MT807921	MT809091
	ME.007.4	MT809068	MT809080	MT807922	MT809092
	ME.007.5			MT807923	MT809093
	PL.015.1	MT809074	MT809086		MT809100
	PL.015.2		MT809087	MT807933	MT809101
	PL.015.3			MT807934	
	PL.015.4			MT807935	MT809102
	US.057.1	MT809072	MT809084	MT807927	MT809098
	US.057.2	MT809073	MT809085		
	US.057.3			MT807928	MT809099
	US.057.4				MT809097

that extract maximum variability uncorrelated with the first component. PC1 extracts the most variance and PC2 extracts less (Tabachnick and Fidell 2007). A one-way ANOVA was used to calculate differences between the paired species based on the results of PCA. The data for the animal and egg PCAs were analysed using OriginPro 2022 software to visualize it appropriately.

RESULTS

Phylogenetic analysis

The ML phylogenetic reconstructions yielded a topology (Fig. 1) with five well-supported clades: the first clade comprised all sequences of *Macrobiotus ripperi* Stec et al. (2021b) (the Polish (PL) and Finnish (FI) population); the second contained all sequences of *Macrobiotus pallarii* Maucci (1954) (the Italian (IT) population); the third contained sequences of *Macrobiotus pseudopallarii* Stec et al. (2021b) (the Montenegrin (ME) population); and the fourth contained sequences of *Macrobiotus margoae* Stec et al. (2021b) (the US populations); and the fifth contained sequences from the Chinese (CN) population (obtained in this study).

Species delimitation

The ASAP results from the *COI* marker are shown in figure 1. The applied ASAP procedure identified five MOTUs (hypothetical species) at the threshold distance of 9.15% (K2P) with the best ASAP-score (1.50) within the available molecular data: *M. ripperi*, *M. pallarii*, *M. pseudopallarii*, *M. margoae*, and a fifth putative species represented by Chinese population analyzed in this study. At the threshold distance of 0.16% (K2P) (but with a poorer ASAP-score of 6.00), the ASAP analysis retrieved nine species (*M. ripperi* was delimited as three species, *M. pseudopallarii* as two species, and a putative species represented by Chinese population analyzed in this study as two species); however, we did not consider this result to be valid, as the lower the ASAP result is scored, the better the partition.

Morphometric analysis

A plot of PC1 and PC2 for the animal and egg measurements is also shown in figure 2. The PCA

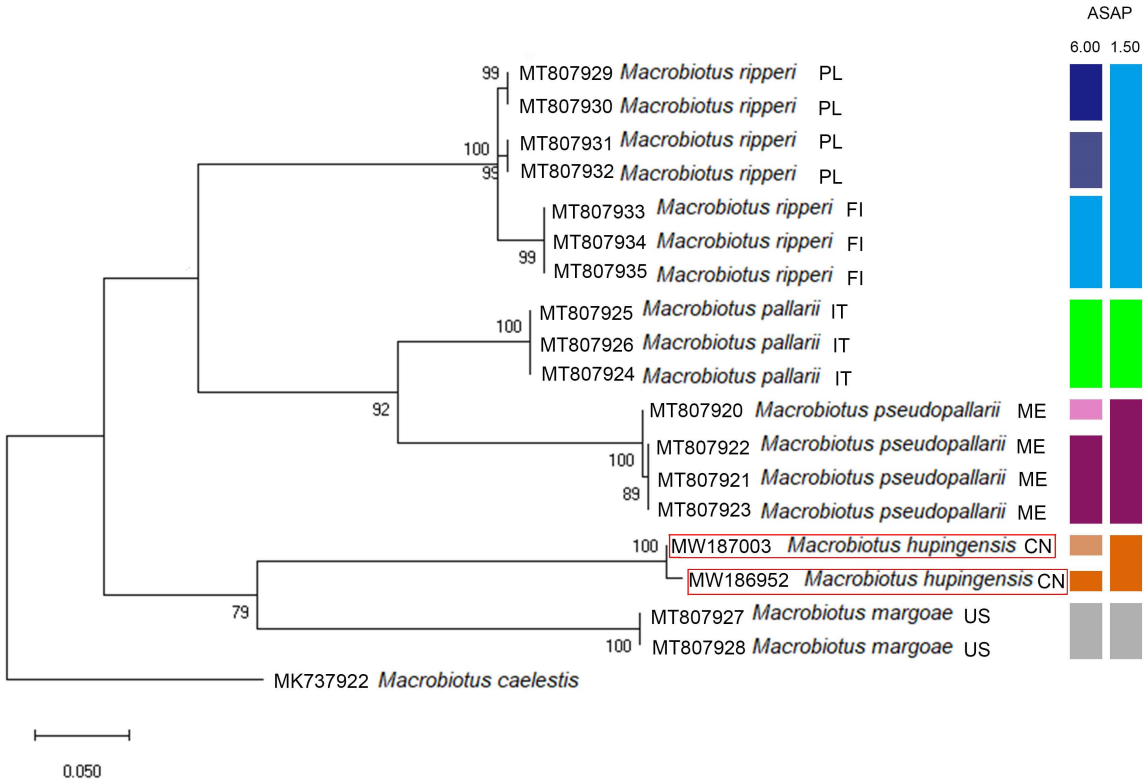

Fig. 1. Maximum Likelihood tree of the *Macrobiotus pallarii* complex, obtained from 19 nucleotide *COI* sequences. Bootstrap values > 50% are provided at major nodes for ML tree calculation methods. The results of species delimitation are indicated by vertical bars. Sequences generated in the course of the present study are given in red box line.

for the animal measurements extracted five principal components, from which PC1 explained 50.6% of the total variation and PC2 explained 8.3%.

ANOVA showed that species identity had an overall significant effect on the PCs ($p < 0.001$, Table 4). Most post hoc pairwise one-way ANOVA comparisons were significant (Table 4); however, the species could not be separated by any of the analysed traits (Fig. 2A), a conclusion that was also supported by low R^2 values (Table 4), thus making morphometric indices impractical for traditional species identification. The only exception was between two groups of populations (*M. pallarii* + *M. ripperi* vs *M. margoae* + *M. pseudopallarii* + the new species analyzed in this study) that showed some separation between the first and second PCs (Fig. 2A). According to the loading plot of PC1 and PC2 (Fig. 2A), the separation between these two groups was driven mainly by the *pt* indices related to the buccal apparatus structures. The PCA for the egg measurements extracted six principal components, from which PC1 explained 50.8% of the total variation and PC2 explained 18.3%. One-way ANOVA showed that the species had an overall significant effect on the PCs ($p < 0.001$, Table 4). All the post hoc pairwise one-way ANOVA comparisons, except *M. pallarii* vs *M. ripperi* (probably due to the big different sample sizes for the two species (10 vs 60, respectively)), were significant (Table 4). However, like animal traits, egg measurements did not distinguish the analysed species (Table 5, Fig. 2B).

Table 4. Results of one-way ANOVA and post hoc pairwise one-way ANOVA comparisons for the first two principal components (PCs) of animal *pt* values; significant post hoc *p*-values at the α-level of $p < 0.045$ are in bold

Term			*d.f.*	SS	F	R^2	*p*
Species			4	5588.01	79.697	0.676	< 0.001
Residuals			154	2681.91		0.324	
Total			158	8269.92		1	
Post hoc comparisons							
M. pallarii	vs	*M. ripperi*	1	25.70	1.09	0.02	0.30
M. ripperi	vs	*M. pseudopallarii*	1	218.09	19.98	0.19	**< 0.001**
M. ripperi	vs	*M. margoae*	1	1760.22	121.93	0.58	**< 0.001**
M. ripperi	vs	*M. hupingensis* sp. nov.	1	3090.58	208.39	0.70	**< 0.001**
M. pseudopallarii	vs	*M. margoae*	1	2413.11	126.45	0.69	**< 0.001**
M. pseudopallarii	vs	*M. hupingensis* sp. nov.	1	3712.99	188.64	0.77	**< 0.001**
M. pallarii	vs	*M. pseudopallarii* sp. nov.	1	139.33	7.50	0.17	**0.01**
M. pallarii	vs	*M. margoae*	1	402.88	14.83	0.29	**< 0.001**
M. pallarii	vs	*M. hupingensis* sp. nov.	1	769.28	27.34	0.43	**< 0.001**
M. margoae	vs	*M. hupingensis* sp. nov.	1	139.50	5.57	0.09	**0.02**

Table 5. Results of one-way ANOVA and post hoc pairwise one-way ANOVA comparisons for the first two principal components (PCs) of egg measurements; significant post hoc *p*-values at the α-level of $p < 0.040$ are in bold

Term			*d.f.*	SS	F	R^2	*p*
Species			4	1093.40	77.00	0.668	**< 0.001**
Residuals			154	543.17		0.332	
Total			158	1636.6		1	
Post hoc comparisons							
M. pallarii	vs	*M. ripperi*	1	0.08	0.04	0.00	0.84
M. ripperi	vs	*M. pseudopallarii*	1	75.87	30.51	0.26	**< 0.001**
M. ripperi	vs	*M. margoae*	1	43.83	16.58	0.16	**< 0.001**
M. ripperi	vs	*M. hupingensis* sp. nov.	1	783.75	198.46	0.69	**< 0.001**
M. pseudopallarii	vs	*M. margoae*	1	173.66	50.85	0.48	**< 0.001**
M. pseudopallarii	vs	*M. hupingensis* sp. nov.	1	278.95	51.95	0.47	**< 0.001**
M. pallarii	vs	*M. pseudopallarii*	1	31.35	12.44	0.25	**0.001**
M. pallarii	vs	*M. margoae*	1	14.83	5.12	0.12	**0.03**
M. pallarii	vs	*M. hupingensis* sp. nov.	1	303.06	51.31	0.58	**< 0.001**
M. margoae	vs	*M. hupingensis* sp. nov.	1	875.53	153.23	0.73	**< 0.001**

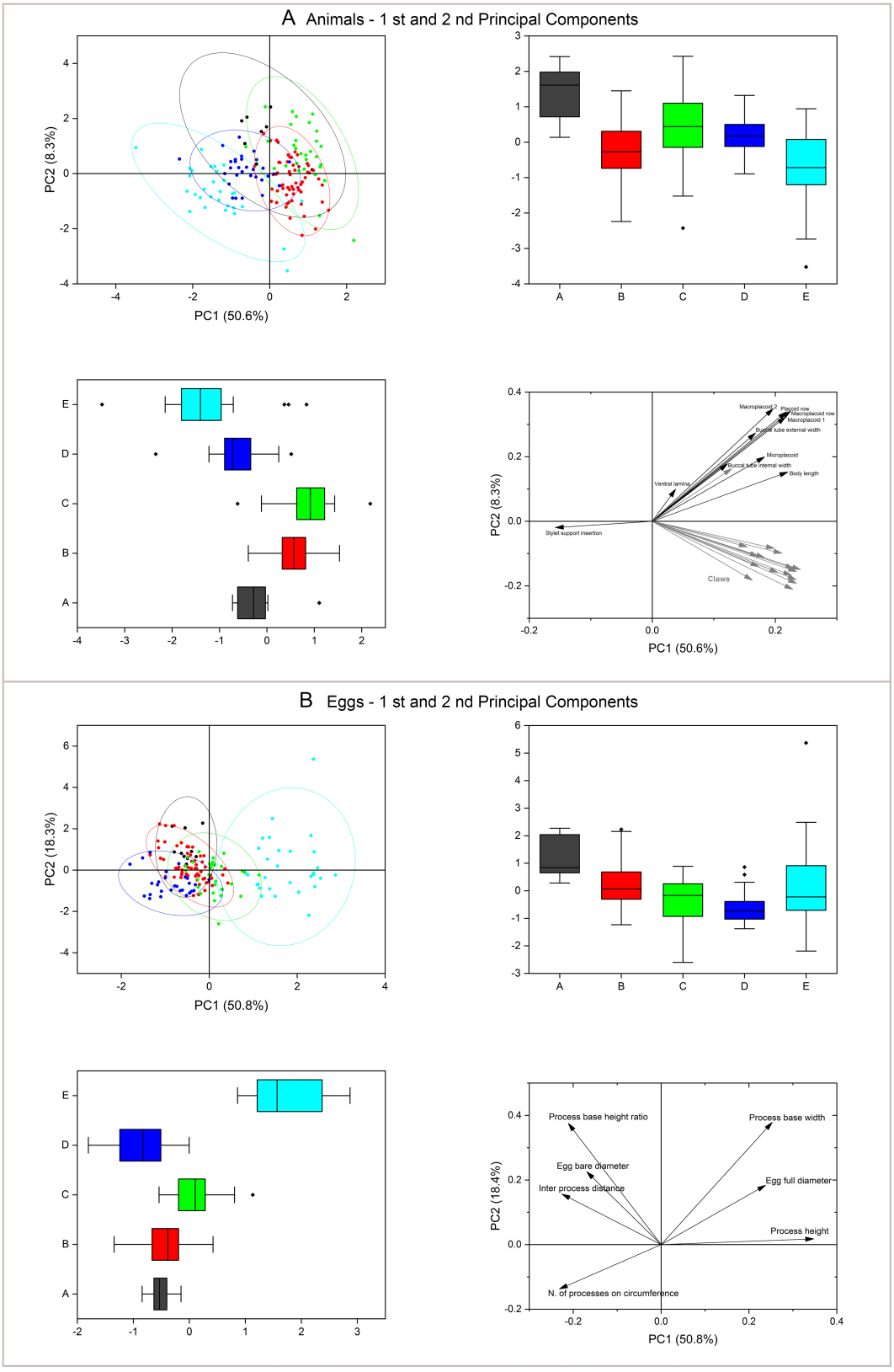

Fig. 2. Results of PCA of animal pt indices and egg raw measurements. A, Animal *pt* indices, 1st and 2nd Principal Components; B, Egg measurements, 1st and 2nd Principal Components; Top-left quadrants: score scatter plots; Top-right quadrants: long plot; bottom-left and right quadrants: boxplots of single component scores.

TAXONOMY

Phylum: Tardigrada Doyère, 1840
Class: Eutardigrada Richters, 1926
Order: Parachela Schuster et al., 1980
Superfamily: Macrobiotoidea Thulin, 1928 (Marley et al. 2011)
Family: Macrobiotidae Thulin, 1928
Genus: Macrobiotus C.A.S. Schultze, 1834

Macrobiotus hupingensis sp. nov.

urn:lsid:zoobank.org:act:DF765A1E-F6C6-4044-AE8B-17FAF9D648F2

Etymology: This species is named after the type locality.

Material examined: 238 animals and 46 eggs. Specimens mounted on microscope slides in Hoyer's medium (223 animals + 42 eggs), fixed on SEM stubs (11 + 4), and processed for DNA sequencing (4 + 0).

Type locality: 30°02'19.1"N, 110°54'45.2"E, 1,065 m asl, the Hupingshan National Nature Reserve, Shimen Country, Hunan Province, China.

Type repository: Holotype (Slide hp1110202 with 29 paratypes), 183 paratypes (Slides: hp I. II. 02. III, the Roman numerals can be substituted by the following numbers: 1–5, 01–25, 1–10, respectively; SEM stub: 11.02) and 40 eggs (slides: hp–I. II. 02. III; SEM stub: 11.02) were deposited at Xiaochen Li's tardigrade collection, Molecular Ecology, Department of Biology, College of Life Sciences of Shaanxi Normal University, China. Additional paratypes (10 animals) (slides: Slides: hp 2. II. 02. III, the Roman numerals II–III can be substituted by the following numbers: 01–25, 1–10) and 6 eggs (slides: hp–I. II. 02. III) are deposited at the Department of Invertebrate Evolution, Institute of Zoology and Biomedical Research, Faculty of Biology, Jagiellonian University, Poland.

Description of the new species: Animals (measurements and statistics in Table 6): In live animals, body almost transparent in smaller specimens and whitish in larger animals; transparent after fixation in Hoyer's medium (Fig. 3). Eyes present in live animals and after fixation in Hoyer's medium. Small round and oval cuticular pores (0.5–1.5 µm in diameter) visible under both PCM and SEM scattered randomly throughout the entire body (Figs. 4A–D, 5A–D). Patches of fine granulation on the external surface of legs I–III as well as on the dorsal and dorsolateral sides of leg IV visible in PCM (Fig. 4B, D) and SEM (Fig. 5B, D). Only pulvinus is present on the internal surface of legs I–III whereas the granulation on the internal surface is absent (Figs. 4C, 5C). In addition to the typical patches of leg granulation, other types of cuticular granulation are absent.

Claws slender, of the *hufelandi* type. Primary branches with distinct accessory points, a long common tract, and an evident stalk connecting the claw to the lunula (Fig. 6A–B, 6D–E). Lunulae on legs I–III smooth, whereas on legs IV usually clearly dentate (Fig. 6A–F). Dark areas under each claw on legs I–III are often visible in PCM (Fig. 6A). Paired muscle attachments and faintly visible continuous cuticular bars above them on legs I–III are often visible both with PCM and SEM (Fig. 6A, D), whereas the horseshoe-shaped structure connecting anterior and posterior claw IV is visible only in PCM (Fig. 6B–C).

Mouth antero-ventral: Buccal apparatus of the *Macrobiotus* type (Fig. 7A), with the ventral lamina and ten peribuccal lamellae (Fig. 8A–B). The oral cavity armature (OCA) was well developed and composed of three bands of teeth, from which only the second and third bands were always clearly visible under PCM (Fig. 7B–C), whereas the first band was only visible under SEM (Fig. 8A–B). The first band of teeth is composed of numerous small teeth visible under SEM as cones (Fig. 8A–B), arranged in several rows, situated anteriorly in the oral cavity, just behind the bases of the peribuccal lamellae. The second band of teeth is situated between the ring fold and the third band of teeth and comprises 3–4 rows of teeth visible with PCM as granules (Fig. 7B–C), and as cones in SEM (Fig. 8A–B) but larger than those in the first band. The posterior row of teeth within the second band seems to comprise larger teeth than the previous anterior rows (Fig. 8A–B). The teeth of the third band are located within the posterior portion of the oral cavity, between the second band of teeth and the buccal tube opening (Figs. 7B–C, 8A–B). The third band of teeth is divided into the dorsal and ventral portions. Under PCM, the dorsal teeth are seen as three distinct transverse ridges, whereas the ventral teeth appear as two separate lateral transverse ridges, between which one large tooth (circular in PCM) is visible (Fig. 7B–C). Pharyngeal bulb spherical, with triangular apophyses, two rod-shaped macroplacoids (2 < 1) and a microplacoid positioned close to them (*i.e.*, the distance between the second macroplacoid and the microplacoid is shorter than the microplacoid length; Fig. 7A, D). The first macroplacoid is anteriorly narrowed and constricted in the middle, whereas the second has a subterminal constriction (Fig. 7D–E).

Eggs (measurements and statistics in Table 7): Laid freely, white, spherical with conical processes surrounded by one row of areolae (Fig. 9A–B). In SEM, multiple rings of faintly visible annulation were visible on the entire process (Fig. 10B, E), although in some processes, annulation was present only in the upper portion of the process (Fig. 10A–F) (annulation

not visible in PCM because it was obscured by the eminent labyrinthine layer). The upper parts of the processes are smooth and not covered with granulation (Fig. 10B, C, E–F). The labyrinthine layer between the process walls is present and visible as reticulation with circular/ellipsoidal meshes throughout the entire process (Figs. 9A–B, 10A–F). Small areas without reticulation are rarely present in some processes (Fig. 9B). The upper part of the process is often elongated into short flexible apices (Figs. 9C–F, 10A–C, E–F), which are occasionally absent or bifurcated and sometimes have bubble-like structures (Figs. 9C–F, 10A–F). The base of the processes extends into the six (only sometimes five) arms that form areolae rims (Fig. 9A–B). Each process is surrounded by six (only sometimes five) hexagonal areolae (Figs. 9A–B, 10A–C), which are occasionally falsely subdivided in the middle into two areolae by a thin thickening perpendicular to the process base (Figs. 9A–B, 10B). Areolae rims (walls) thick and usually flat (Fig. 10A, C), with the labyrinthine layer inside the rims visible as bubbles in PCM (Fig. 9B). Areolae rims also delimit the areolae at the bases of processes, which forms an irregular collar around process bases (Figs. 9B, 10A, C) and makes the process bases penta- or hexagonal in the top view (Figs. 9A–B, 10A–C). The areola surface has wrinkles that are faintly visible under PCM (Fig. 9A–B) but clearly visible under SEM (Fig. 10B–D). Micropores are present within the areolae,

Table 6. Measurements and *pt* values of selected morphological structures of the holotype and paratypes of *Macrobiotus hupingensis* sp. nov.

Character	N	Range		Mean		SD		Holotype	
		µm	*pt*	µm	*pt*	µm	*pt*	µm	*pt*
Body length	30	307–496	*794–1151*	371	*945*	49	*91*	426	*1078*
Buccal tube									
Buccal tube length	30	31.7–54.2	–	39.3	–	4.4	–	39.5	–
Stylet support insertion point	30	24.7–43.6	*77.5–81.9*	31.4	*80.0*	3.6	*1.2*	31.9	*80.8*
Buccal tube external width	30	3.5–7.2	*9.6–16.6*	5.3	*13.4*	0.9	*1.7*	5.4	*13.7*
Buccal tube internal width	30	2.6–6.3	*7.1–16.3*	4.2	*10.7*	0.8	*1.8*	4.2	*10.6*
Ventral lamina length	30	17.2–34.8	*50.7–65.7*	23.1	*58.7*	3.4	*5.5*	25.4	*64.3*
Placoid lengths									
Macroplacoid 1	30	4.6–11.1	*13.0–29.3*	7.3	*18.7*	1.4	*3.2*	8.1	*20.5*
Macroplacoid 2	30	3.9–7.8	*11.3–18.4*	5.9	*15.1*	0.9	*1.6*	6.3	*15.9*
Microplacoid	30	1.9–3.4	*4.8–8.4*	2.5	*6.3*	0.4	*1.0*	2.9	*7.3*
Macroplacoid row	30	10.6–18.8	*29.9–45.4*	14.8	*37.8*	2.1	*3.9*	16.0	*40.5*
Placoid row	29	15.9–27.3	*47.1–55.3*	20.0	*51.2*	2.4	*1.8*	20.5	*51.9*
Claw I heights									
External primary branch	29	7.2–11.1	*15.9–29.3*	8.9	*22.7*	1.0	*3.0*	8.4	*21.3*
External secondary branch	27	5.7–9.7	*13.8–25.6*	7.2	*18.4*	0.9	*2.5*	7.2	*18.2*
Internal primary branch	30	6.6–10.4	*16.6–28.1*	8.6	*22.0*	0.8	*2.6*	8.3	*21.0*
Internal secondary branch	29	5.4–8.6	*13.1–22.7*	6.8	*17.3*	0.7	*1.8*	6.5	*16.5*
Claw II heights									
External primary branch	30	7.9–11.8	*17.9–32.8*	9.2	*23.6*	0.9	*3.3*	8.4	*21.3*
External secondary branch	30	4.8–11.0	*12.2–29.0*	7.2	*18.4*	1.1	*3.0*	7.2	*18.2*
Internal primary branch	30	7.4–10.6	*16.8–32.8*	8.8	*22.7*	1.0	*3.2*	8.1	*20.5*
Internal secondary branch	29	5.7–8.8	*13.5–22.0*	7.0	*17.9*	0.9	*2.1*	7.1	*18.0*
Claw III heights									
External primary branch	29	7.1–11.7	*19.4–33.4*	9.5	*24.4*	1.0	*3.3*	8.7	*22.0*
External secondary branch	29	5.4–8.2	*12.7–24.9*	7.1	*18.2*	0.8	*2.7*	7.4	*18.7*
Internal primary branch	30	7.1–10.6	*18.3–29.1*	9.0	*23.2*	0.8	*2.7*	8.7	*22.0*
Internal secondary branch	27	5.5–9.0	*13.1–23.7*	7.3	*18.9*	0.8	*2.3*	7.3	*18.5*
Claw IV heights									
Anterior primary branch	30	8.5–13.7	*22.3–35.7*	10.7	*27.3*	1.3	*3.2*	10.9	*27.6*
Anterior secondary branch	30	5.7–10.2	*14.9–25.6*	8.0	*20.4*	1.2	*2.7*	9.2	*23.3*
Posterior primary branch	30	9.5–13.0	*20.3–35.3*	11.1	*28.4*	1.0	*3.3*	10.6	*26.8*
Posterior secondary branch	28	6.2–11.2	*13.5–29.6*	8.1	*20.8*	1.1	*2.8*	8.1	*20.5*

N = number of specimens/structures measured; Range = the smallest and the largest structure among all measured specimens; SD = standard deviation.

but they are distributed only around the areolae rims and usually absent in the central part of the areola (Fig. 10B–D).

Remarks: The wall of egg processes is perforated with a small number pores, which can only be seen in SEM (Fig. 10C–F).

Reproduction: The species is dioecious. Spermathecae in females as well as testes in males have been found to be filled with spermatozoa, clearly visible under PCM up to 24 hours after mounting in Hoyer's medium (Fig. 11A–B). The species exhibits secondary sexual dimorphism in the form of clearly visible lateral gibbosities on hind legs in males (Fig. 11B).

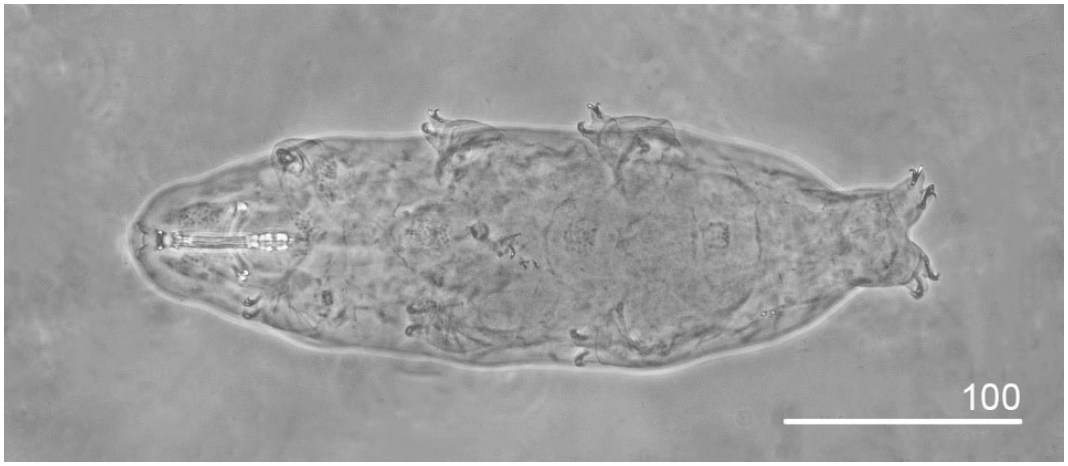

Fig. 3. *Macrobiotus hupingensis* sp. nov. from China seen in PCM (holotype, Hoyer's medium) – habitus, adult specimen in dorso-ventral projection. Scale bar in µm.

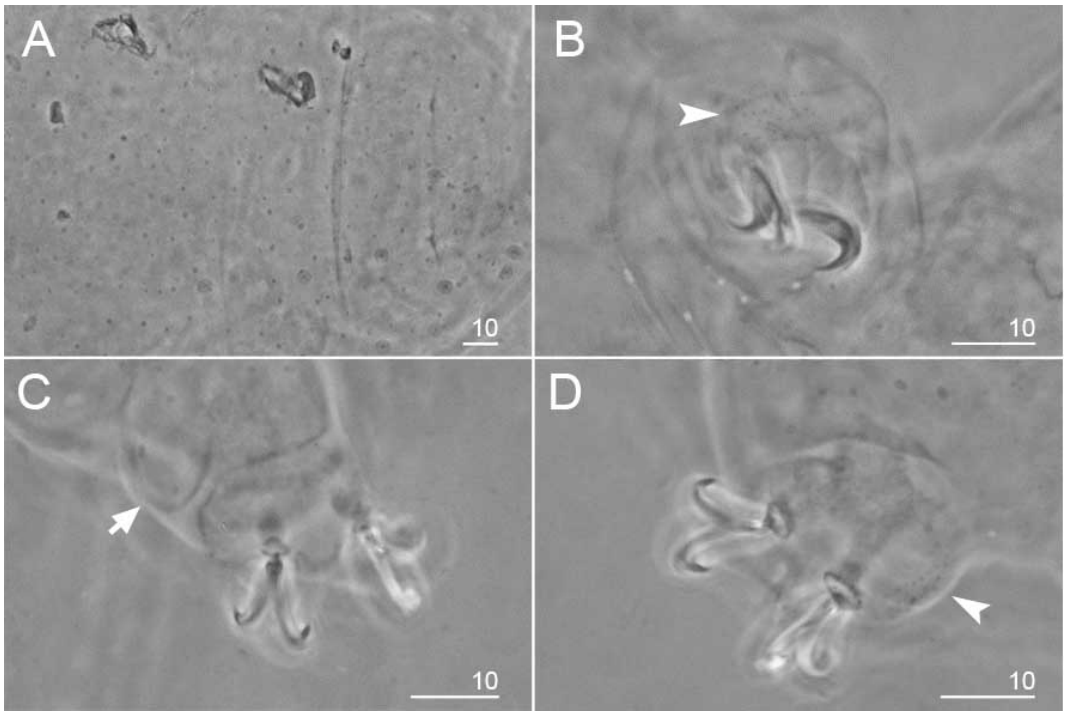

Fig. 4. *Macrobiotus hupingensis* sp. nov. from China seen in PCM (paratypes) – body and leg cuticle morphology seen with PCM: A, cuticle on the last body segment without caudal band of granulation; B, granulation on the external surface of leg II; C, internal surface of leg III with evident pulvinus; D, granulation on dorsal surface of leg IV. Filled indented arrowheads indicate granulation on the legs, arrow indicates pulvinus on the III leg. Scale bar in µm.

DNA sequences and intraspecific genetic distances

We obtained sequences for all four molecular markers amplified in this study. All sequenced fragments were represented by two haplotypes except the 18S rRNA, in which only one single haplotype was present:

18S rRNA sequences (GenBank: MW183923); 1749 bp long; 1 haplotype was found.

28S rRNA sequences (GenBank: MZ470349–50); 811 bp long; 2 haplotypes were found, separated by a *p*-distance of 0.1%.

ITS-2 sequences (GenBank: MZ474842–3); 432 bp long; 2 haplotypes were found, separated by a *p*-distance of 0.2%.

COI sequences (GenBank: MW186952 and MW187003); 684 bp long; 2 haplotypes were found, separated by a *p*-distance of 0.8%.

DISCUSSION

Phenotypic differential diagnosis

The processes of *M. hupingensis* sp. nov. are surrounded by 5–6 areolae, resembling five other species in the *Macrobiotus pallarii* complex. Based on the morphology of the animals and eggs, this species

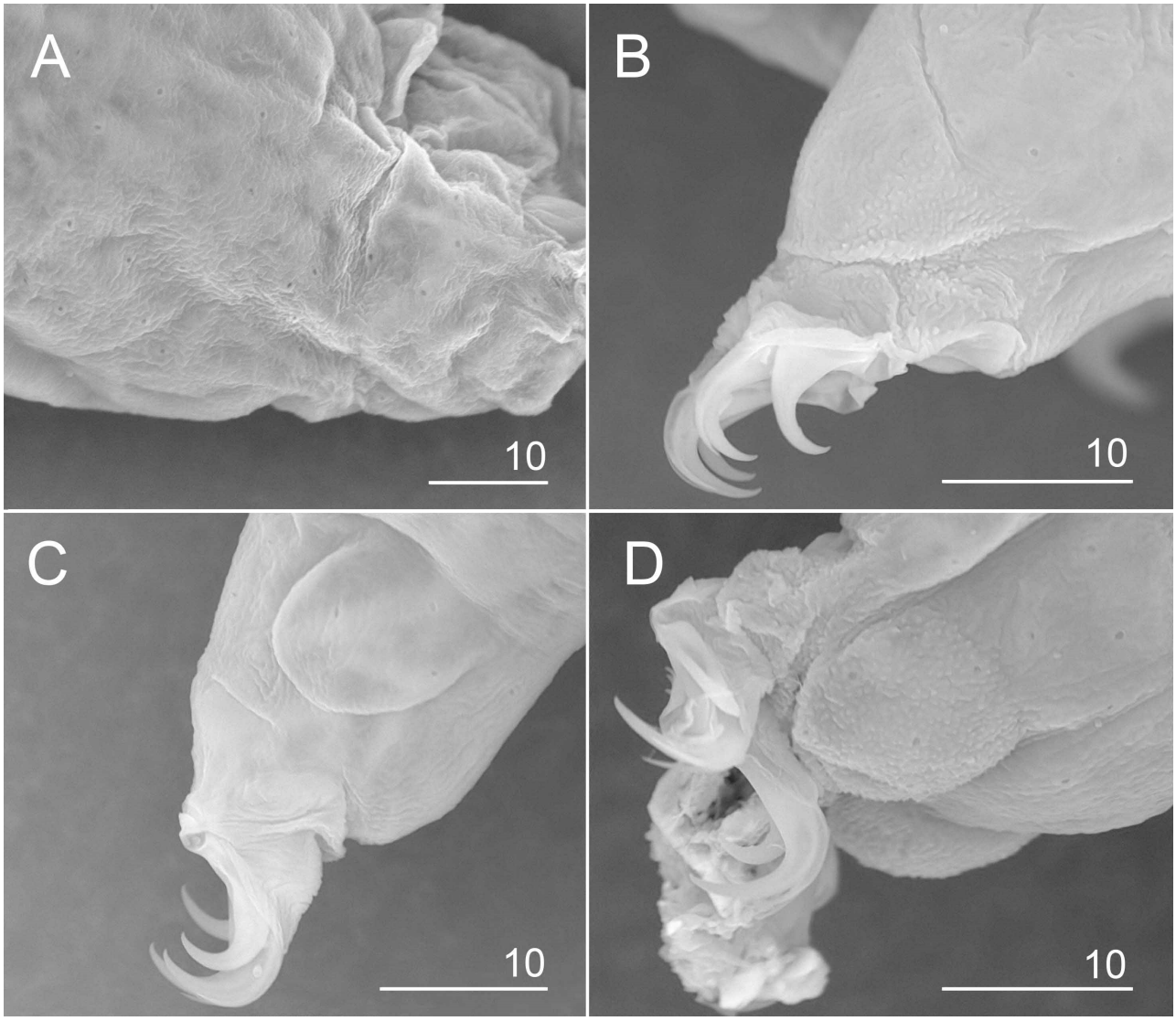

Fig. 5. *Macrobiotus hupingensis* sp. nov. from China seen in SEM (paratypes) – body and leg cuticle morphology seen with SEM: A, cuticle on the last body segment without caudal band of granulation; B, granulation on the external surface of leg III; C, internal surface of leg II with evident pulvinus; D, granulation on dorsal surface of leg IV. Scale bar in μm.

can be differentiated from the following (Stec et al. 2021b):

Macrobiotus pallarii: by a weakly developed oral cavity armature, with the first band of teeth not visible under PCM (the oral cavity armature is well developed, and the first band of teeth is visible under PCM in *M. pallarii*), by dentate lunulae IV (lunulae are faintly crenulated in *M. pallarii*), by the absence of two lateral patches of dense granulation between legs III and IV (dense granulation patches between legs III and IV are present in *M. pallarii*), by the absence of a sparse dorsal granulation between legs III and IV (sparse granulation is present in *M. pallarii*), by a lower placoid row *pt* value (*47.1–55.3* in *Macrobiotus hupingensis* sp. nov. vs. *61.3–75.6* in *M. pallarii*), by the absence of granulation on the egg processes tips (granulation is present in *M. pallarii*; character visible only under SEM), and by more developed and better visible micropores within the areoles in SEM.

Macrobiotus pseudopallarii: by a weakly developed oral cavity armature, with the first band of teeth not visible under PCM (the oral cavity armature is well developed, and the first band of teeth is visible under PCM in *M. pseudopallarii*), by dentate lunulae IV (lunulae are gently dentate in *M. pseudopallarii*), by the absence of two lateral patches of dense granulation between legs III and IV (the dense granulation patches between legs III and IV are present in *M. pseudopallarii*; see Fig. 1), by the absence of sparse dorsal granulation between legs III and IV (the sparse granulation is present in *M. pseudopallarii*), by a lower placoid row *pt* value (*47.1–55.3* in *Macrobiotus hupingensis* sp. nov. vs. *65.0–75.1* in *M. pseudopallarii*), by the absence of granulation on the egg processes tips (granulation is present in *M. pseudopallarii*; character visible only under SEM), and by more developed and better visible micropores within the areoles in SEM.

Macrobiotus ripperi: by a weakly developed oral cavity armature, with the first band of teeth not visible under PCM (the oral cavity armature is well developed, and the first band of teeth is visible under PCM in *M. ripperi*), by the absence of sparse dorsal granulation between legs III and IV (sparse granulation is present in *M. ripperi*), and by more developed and better visible micropores within the areoles in SEM.

Macrobiotus margoae: by the presence of meshes within the entire process walls (only small circular bubbles scattered randomly within the process are found

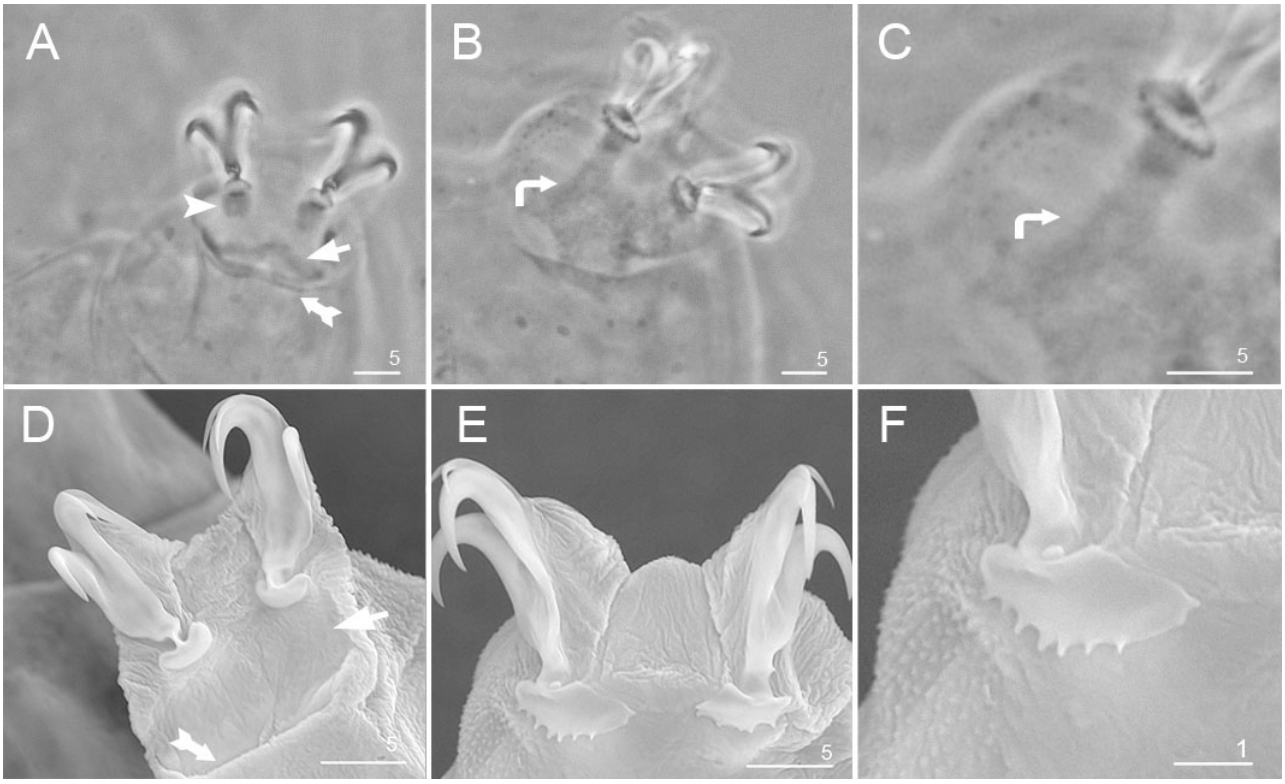

Fig. 6. *Macrobiotus hupingensis* sp. nov. from China (paratypes) – claw morphology: A–B, claws II and IV seen with PCM; C, magnification of lunulae IV seen with PCM; D–E, claws I and IV seen with SEM; F, magnification of lunulae IV seen with SEM. Indented arrowhead indicates dark circular areas under lunulae on the first three pairs of legs, double arrowheads indicate double muscle attachments under claws, arrows indicate cuticular bar above muscle attachments, bent arrows indicate horseshoe structure connecting the anterior and the posterior claw. Scale bars in µm.

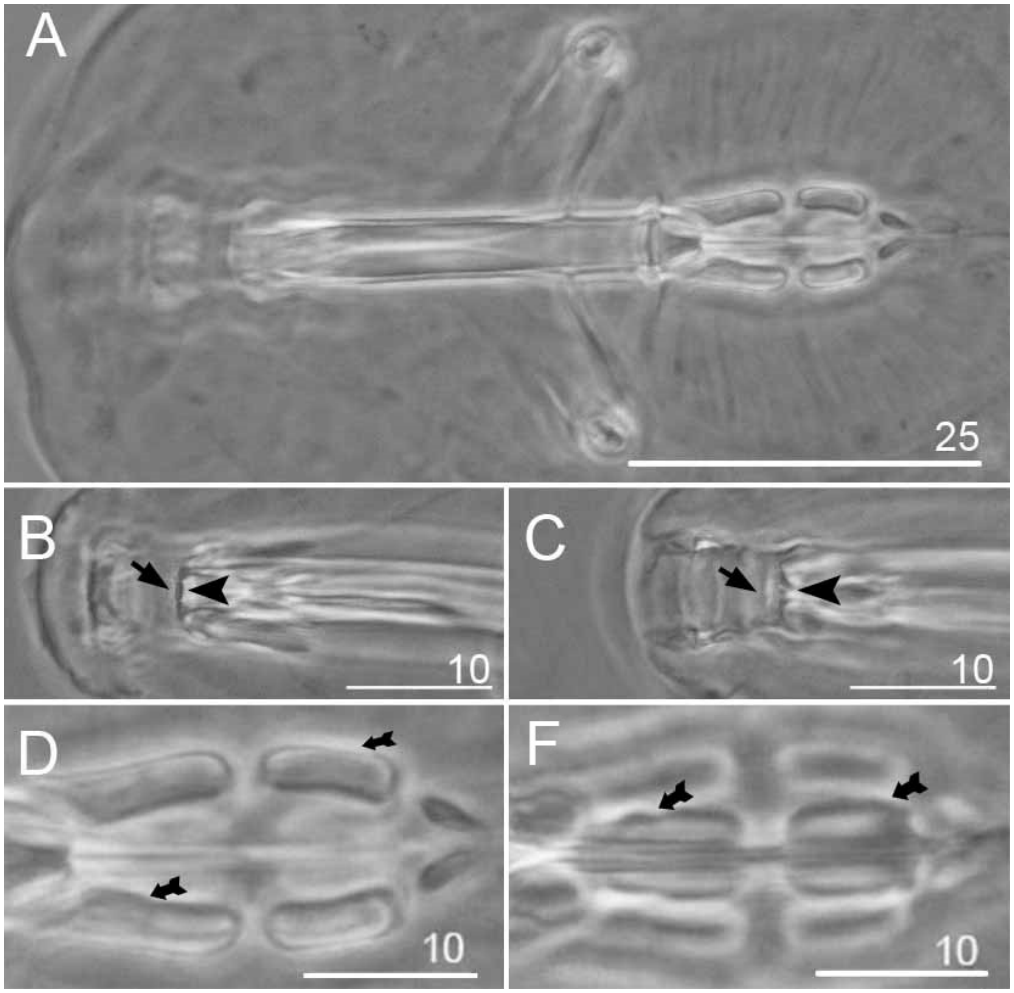

Fig. 7. *Macrobiotus hupingensis* sp. nov. from China (paratype) – buccal apparatus seen with PCM: A, an entire buccal apparatus; B–C, the oral cavity armature, dorsal and ventral teeth, respectively; D–E, placoid morphology, dorsal and ventral placoids, respectively. Arrows indicate the second band of teeth, indented arrowheads indicate the third band of teeth, double arrowhead indicates central and subterminal constrictions in the first and second macroplacoid. Scale bars in µm.

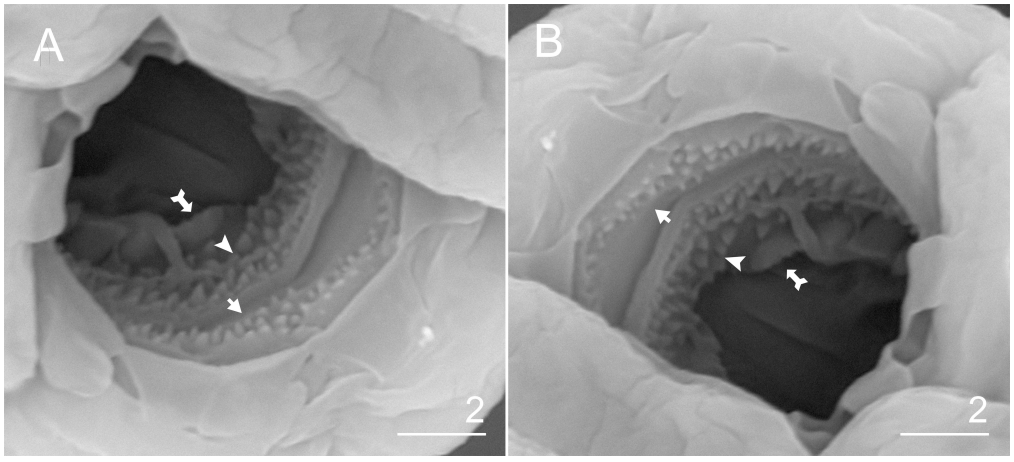

Fig. 8. *Macrobiotus hupingensis* sp. nov. from China (paratype) – the oral cavity armature seen with SEM: A–B, the oral cavity armature of a single specimen seen with SEM from different angles showing dorsal and ventral portion, respectively. Arrows indicate the first band of teeth, indented arrowheads indicate the second band of teeth, double arrowhead indicates the third band of teeth. Scale bars in µm.

in *M. margoae*). (Remarks: The putative character that might be used to discriminate between these two species is the presence (new species) vs. absence (*M. margoae*) of pores in the egg processes walls. However, the validity of such distinction should be treated with a dose of caution since usually the number of eggs imagined in SEM is not very large, preventing proper verification of this trait variability).

Macrobiotus caymanensis (known only from the Cayman Islands): by the presence of granulation visible with PCM on all legs (leg granulation is absent or not visible under PCM in *M. caymanensis*), by lunulae IV being dentate (the lunulae are smooth in *M. caymanensis*), by the presence of meshes within

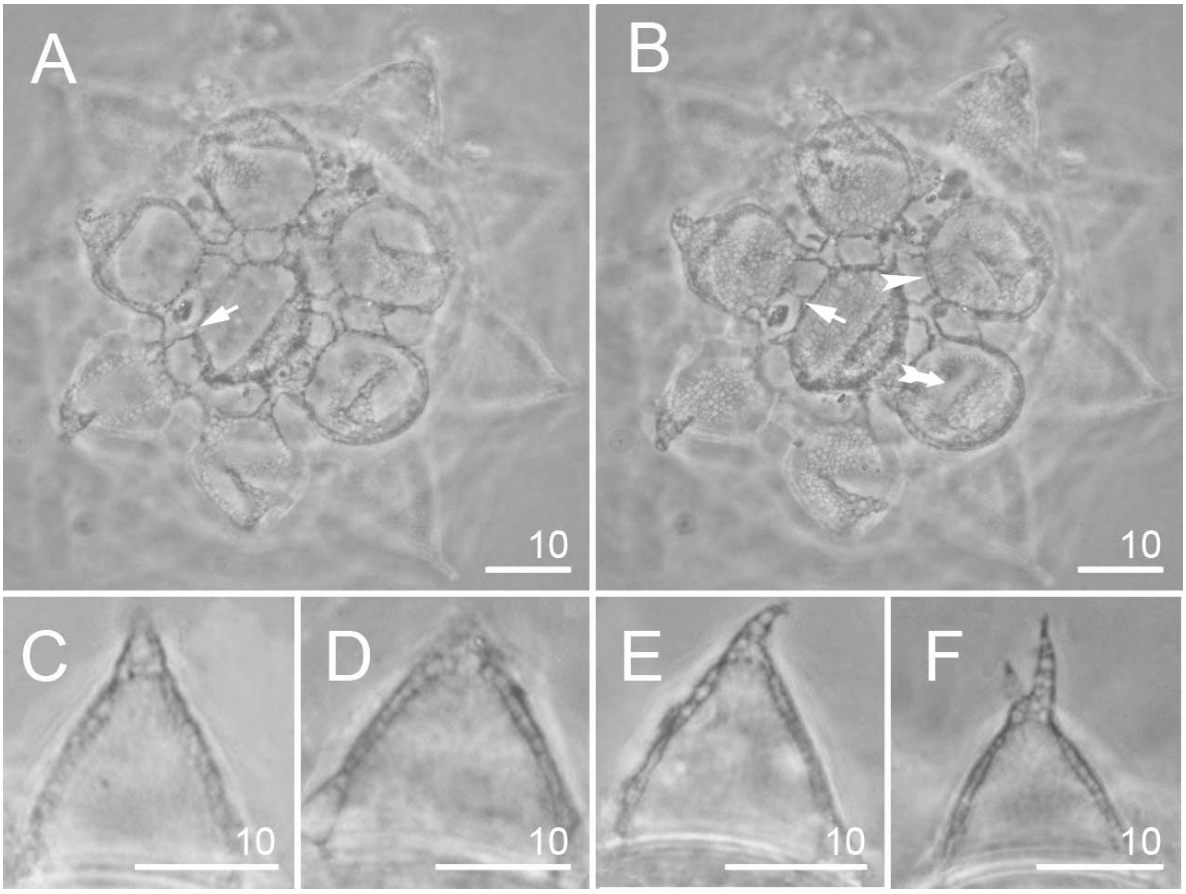

Fig. 9. *Macrobiotus hupingensis* sp. nov. from China (paratypes) – eggs seen with PCM: A–B, surface under ×1000 magnification of egg; C–F, midsections of four different egg processes. Arrows indicate thickening perpendicular to the process base that divides the areola in the middle, double arrowhead indicates areas of the egg processes without reticulation/labyrinthine layer, and indented arrowheads indicate irregular collar around process bases. Scale bars in µm.

Table 7. Measurements (µm) and quantitative characters of eight measurable eggs of *Macrobiotus hupingensis* sp. nov.

Character	N	Range	Mean	SD
Egg bare diameter	30	52.4–73.2	62.2	6.4
Egg full diameter	25	85.9–127.6	107.1	12.8
Process height	90	17.1–30.9	24.0	4.1
Process base width	90	15.0–37.5	20.4	3.9
Process base/height ratio	90	53%–134%	87%	17%
Inter-process distance	90	1.9–6.5	3.6	1.0
Number of processes on the egg circumference	28	9–10	9.5	0.5

N = number of eggs/structures measured. Range = the smallest and the largest structure among all measured specimens. SD = standard deviation.

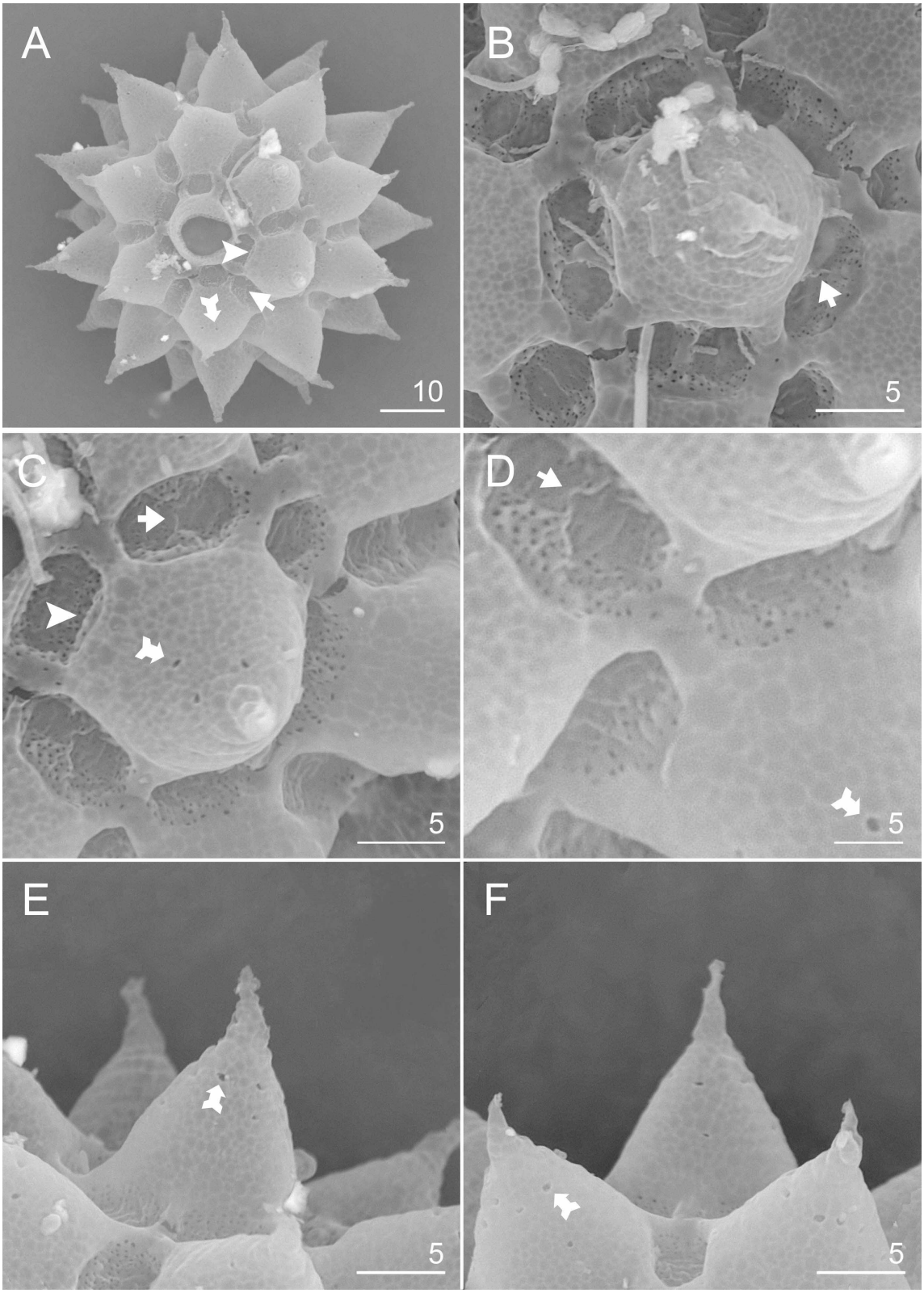

Fig. 10. *Macrobiotus hupingensis* sp. nov. from China (paratypes) – eggs seen with SEM: A, entire view of the egg (missing a process); B–F, details of the egg surface between processes, areolation and egg processes. The arrows indicate thickening perpendicular to the process base, which divides the areola in the middle, indented arrowheads indicate irregular collar around process bases, and double arrowheads indicate pores on the surface of egg processes. Scale bars in µm.

the entire process wall (only small circular bubbles scattered randomly within the process wall are found in *M. caymanensis*).

Genotypic differential diagnosis

Interspecific uncorrected genetic *p*-distances between *M. hupingensis* sp. nov. and other species in the *M. pallarii* complex are as follows:

18S rRNA: 4.3–4.8% (4.6% on average), with the most similar being *M. margoae* from the USA (MT809072–3) and the least similar being *M. pallarii* from Italy (MT809069–71) and *M. pseudopallarii* from Montenegro (MT809065–7).

28S rRNA: 2.8–3.1% (2.9% on average), with the most similar being *M. pseudopallarii* from Montenegro (MT809077–80) and the least similar being *M. margoae* from the USA (MT809084–5).

ITS-2: 14.5–15.7% (15.2% on average), with the most similar being *M. ripperi* from Finland (MT809100–2) and *M. ripperi* from Poland (MT809103), and the least similar being *M. pseudopallarii* from Montenegro (MT809090–3).

COI: 28.8–37.0% (32.5% on average), with the most similar being *M. margoae* from the USA (MT807927–8) and the least similar being *M. ripperi* from Finland (MT807933–5).

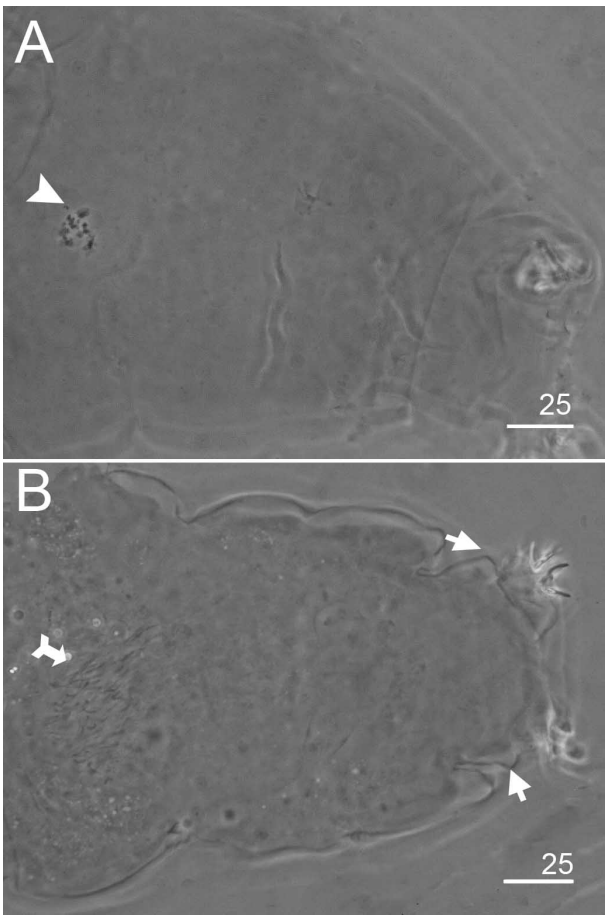

Fig. 11. *Macrobiotus hupingensis* sp. nov. from China (paratypes) – reproduction (PCM): A, spermatheca (seminal vesicle) filled with spermatozoa and visible in females freshly mounted in Hoyer's medium; B, testis filled with sperm visible in a male freshly mounted in Hoyer's medium. The indented arrowhead indicates the female spermathecae, double arrowhead indicates the testis, and the arrows indicate gibbosity on the IV leg. Scale bars in µm.

CONCLUSIONS

Macrobiotus hupingensis sp. nov. is new to science and was identified by integrating phase contrast light microscopy, scanning electron microscopy, and DNA analysis. To the best of our knowledge, 1) this is the 28th *Macrobiotus* species found in China to be reported in a peer-reviewed publication and 2) the number of tardigrade species reported in China is much smaller than those of countries in which tardigrades are more intensively studied, thus the actual number of *Macrobiotus* species in China is likely higher than 28. Importantly, the newly studied population from China stays in the sister relationship with *M. margoe*.

M. pallarii has been recorded from China by Sun (2014), but there is no slide for us to confirm whether the previous record was the species we are currently describing or yet another distinct species of the complex. Only further integrative studies can disentangle this issue with confidence.

Acknowledgment: This work and the new species name were registered with ZooBank under urn:lsid:zoobank.org:pub:A6527143-69CD-4180-8A1C-C9579A486B01. We are thankful to the staff of the Hupingshan National Nature Reserve for their kind help in moss collecting. We are grateful to Ms Bi Rui and Guo Yan for their kind help in specimen sorting and slide mounting. We are especially grateful to Professor Zhaoming Wei and his postgraduate Xiaolan Miao in SEM imaging. We also sincerely thank an anonymous reviewer for their valuable comments and suggestions which greatly improved the manuscript. This work was supported by the Natural Science Foundation of Science and Technology Department of Shaanxi Province, China (No. 2013JM3013 and 2014JM2-3026) and Natural Science Foundation of Education Department of Shaanxi Province, China (No. 16JK1186).

Authors' contributions: Conceived and designed the experiments: ZY and XL. Performed the experiments: ZY, YW, QL and LL. Analyzed the data: ZY and YW.

Wrote the paper: ZY. All authors read and approved the final manuscript.

Competing interests: No potential conflict of interest was reported by the authors.

Availability of data and materials: Sequences generated in the study have been deposited into the GenBank database (accession numbers in Table 3 in manuscript).

Consent for publication: Not applicable.

Ethics approval consent to participate: Not applicable.

REFERENCES

Bertolani R, Guidetti R, Marchioro T, Altiero T, Rebecchi L, Cesari M. 2014. Phylogeny of Eutardigrada: New molecular data and their morphological support lead to the identification of new evolutionary lineages. Mol Phylogenet Evol **76:**110–126. doi:10.1016/j.ympev.2014.03.006.

Bi R. 2019. Study on tardigrada fauna and species diversity in Dabie Mountain area. MSc Thesis, Shaanxi Normal University. (in Chinese)

Cesari M, Giovannini I, Altiero T, Guidetti R, Cornette R, Kikawada T, Rebecchi L. 2022. Resistance to extreme stresses by a newly discovered Japanese Tardigrade species, *Macrobiotus kyoukenus* (Eutardigrada, Macrobiotidae). Insects **13:**634. doi:10.3390/insects13070634.

Chen CD, Li DH. 2003. On the biodiversity and the ecological in tegrity of Wulingyuan district, Hunan Province. Acta Ecologica Sinica **23:**2415–2423. (in Chinese)

Coughlan K, Michalczyk Ł, Stec D. 2019. *Macrobiotus caelestis* sp. nov., a new tardigrade species (Macrobiotidae: *hufelandi* group) from the Tien Shan mountains (Kyrgyzstan). Ann Zool **69:**499–513. doi:10.3161/00034541ANZ2019.69.3.002.

Coughlan K, Stec D. 2019. Two new species of the *Macrobiotus hufelandi* complex (Tardigrada: Eutardigrada: Macrobiotidae) from Australia and India, with notes on their phylogenetic position. Eur J Taxon **573:**1–38. doi:10.5852/ejt.2019.573.

Dastych H. 1980. Niesporczaki (Tardigrada) Tatrzańskiego Parku Narodowego. Monografie Fauny Polski **9:**1–232.

Degma P, Bertolani R, Guidetti R. 2009–2021. Actual checklist of Tardigrada species. Accessed 19 July 2021.

Degma P, Guidetti R. 2007. Notes to the current checklist of Tardigrada. Zootaxa **1579:**41–53. doi:10.11646/zootaxa.1579.1.2.

Edgar R. 2004. MUSCLE: multiple sequence alignment with high accuracy and high throughput. Nucleic Acids Rese **32:**1792–1797. doi:10.1093/nar/gkh340.

Folmer O, Black M, Hoeh W, Lutz R, Vrijenhoek R. 1994. DNA primers for amplification of mitochondrial cytochrome *c* oxidase subunit I from diverse metazoan invertebrates. Mol Mar Biol Biotechnol **3:**294–299.

Gao XY, Li XC, Wang LZ. 2012. Taxonomic composition of the Chinese terrestrial-freshwater tardigrades. J Anhui Agric Sci **40:**9721–9725. (in Chinese)

Gąsiorek P, Stec D, Zawierucha Z, Kristensen RM, Michalczyk Ł. 2018. Revision of *Testechiniscus* Kristensen, 1987 (Heterotardigrada: Echiniscidae) refutes the polar-temperate distribution of the genus. Zootaxa **4472:**261–297. doi:10.11646/zootaxa.4472.2.3.

Greven H. 2018. From Johann August Ephraim Goeze to Ernst Marcus: A Ramble Through the History of Early Tardigrade Research (1773 Until 1929). *In*: Water Bears: The Biology of Tardigrades. Springer, Cham.

Guidetti R, Bertolani R. 2005. Tardigrade taxonomy: an updated check list of the taxa and a list of characters for their identification. Zootaxa **845:**1–46. doi:10.11646/zootaxa.845.1.1.

Guidetti R, Schill, RO, Bertolani R, Dandekar T, Wolf M. 2009. New molecular data for tardigrade phylogeny, with the erection of *Paramacrobiotus* gen. nov. J Zool Sys Evol Res **47:**315–321. doi:10.1111/j.1439-0469.2009.00526.x.

Guo Y. 2020. Study on tardigrada fauna and species diversity in Funiu Mountain area. Mster thesis, Shaanxi Normal University. (in Chinese)

Hall TA. 1999. BioEdit: a user-friendly biological sequence alignment editor and analysis program for Windows 95/98/ NT. Nucleic Acids Symposium Series **41:**95–98.

Kaczmarek Ł, Cytan J, Zawierucha K, Diduszko D, Michalczyk Ł. 2014. Tardigrades from Peru (South America), with descriptions of three new species of Parachela. Zootaxa **3790:**357–379. doi:10.11646/zootaxa.3790.2.5.

Kaczmarek Ł, Michalczyk Ł. 2017. The *Macrobiotus hufelandi* (Tardigrada) group revisited. Zootaxa **4363:**101–123. doi:10.11646/zootaxa.4363.1.4.

Katoh K, Toh H. 2008. Recent developments in the MAFFT multiple sequence alignment program. Brief Bioinform **9:**286–298. doi:10.1093/bib/bbn013.

Katoh K, Misawa K, Kuma K, Miyata T. 2002. MAFFT: A novel method for rapid multiple sequence alignment based on fast Fourier transform. Nucleic Acids Res **30:**3059–3066. doi:10.1093/nar/gkf436.

Kiosya Y, Pogwizd J, Matsko Y, Vecchi M, Stec D. 2021. Phylogenetic position of two *Macrobiotus* species with a revisional note on Macrobiotus sottilei Pilato, Kiosya, Lisi & Sabella, 2012 (Tardigrada: Eutardigrada: Macrobiotidae). Zootaxa **4933:**113–135. doi:10.11646/zootaxa.4933.1.5.

Kumar S, Stecher G, Li M, Knyaz C, Tamura K. 2018. MEGA X: Molecular Evolutionary Genetics Analysis across computing platforms. Mol Bio Evol **35:**1547–1549. doi:10.1093/molbev/msy096.

Lanfear R, Frandsen PB, Wright AM, Senfeld T, Calcott B. 2016. PartitionFinder 2: new methods for selecting partitioned models of evolution for molecular and morphological phylogenetic analyses. Mol Biol Evol **34:**772–773. doi:10.1093/molbev/msw260.

Liu H, Tang DW, Song EP, Chang S. 2020. Spatiotemporal Dynamics of Vegetation net Primary Productivity and Its Driving Factors in Wuling Mountains Areas During 2000–2015. Res Soil Water Conv **27:**218–225. doi:10.13869/j.cnki.rswc.2020.06.029. (in Chinese)

Marley NJ, McInnes SJ, Sands CJ. 2011. Phylum Tardigrada: a re-evaluation of the Parachela. Zootaxa **2819:**51–64. doi:10.11646/zootaxa.2819.1.2.

Michalczyk Ł, Kaczmarek Ł. 2003. A description of the new tardigrade *Macrobiotus reinhardti* (Eutardigrada, Macrobiotidae, *harmsworthi* group) with some remarks on the oral cavity armature within the genus *Macrobiotus* Schultze. Zootaxa **331:**1–24. doi:10.5281/zenodo.156189.

Michalczyk Ł, Kaczmarek Ł. 2013. The Tardigrada Register: a comprehensive online data repository for tardigrade taxonomy. J Limnol **72:**175–181. doi:10.4081/jlimnol.2013.s1.e22.

Michalczyk Ł, Wełnicz W, Frohme M, Kaczmarek Ł. 2012. Redescriptions of three *Milnesium* Doyere, 1840 taxa (Tardigrada: Eutardigrada: Milnesiidae), including the nominal species for the genus. Zootaxa **3154:**120. doi:10.11646/zootaxa.3154.1.1.

Miller MA, Pfeiffer W, Schwartz T. 2010. Creating the CIPRES Science Gateway for inference of large phylogenetic trees. 2010 gateway computing environments workshop (GCE): pp. 1–8. doi:10.1109/GCE.2010.5676129.

Mironov SV, Dabert J, Dabert M. 2012. A new feather mite species of the genus Proctophyllodes Robin, 1877 (Astigmata: Proctophyllodidae) from the Long-tailed Tit Aegithalos caudatus (Passeriformes: Aegithalidae): morphological description with DNA barcode data. Zootaxa **3253:**54–61. doi:10.11646/zootaxa.3253.1.2.

Pilato G. 1981. Analisi di nuovi caratteri nello studio degli Eutardigrada. Animalia **8:**51–57.

Puillandre N, Brouillet S, Achaz G. 2021. ASAP: Assemble species by automatic partitioning. Mol Ecol Resour **21:**609–620. doi:10.1111/1755-0998.13281.

Sands CJ, McInnes SJ, Marley NJ, Goodall-Copestake W, Convey P, Linse K. 2008. Phylum Tardigarda: an "individual" approach. Cladistics **24:**1–18. doi:10.1111/j.1096-0031.2008.00219.x.

Stec D, Dudziak M, Michalczyk Ł. 2020a. Integrative descriptions of two new Macrobiotidae species (Tardigrada: Eutardigrada: Macrobiotoidea) from French Guiana and Malaysian Borneo. Zool Stud **59:**23. doi:10.6620/ZS.2020.59-23.

Stec D, Morek W, Gąsiorek P, Michalczyk Ł. 2018. Unmasking hidden species diversity within the *Ramazzottius oberhaeuseri* complex, with an integrative redescription of the nominal species for the family Ramazzottiidae (Tardigrada: Eutardigrada: Parachela). Syst Biodivers **16:**357–376. doi:10.1080/14772000.2018.1424267.

Stec D, Smolak R, Kaczmarek Ł, Michalczyk Ł. 2015. An integrative description of *Macrobiotus paulinae* sp. nov. (Tardigrada: Eutardigrada: Macrobiotidae: *hufelandi* group) from Kenya. Zootaxa **4052(5):**501–526. doi:10.11646/zootaxa.4052.5.1.

Stec D, Tumanov DT, Kristensen RM. 2020b. Integrative taxonomy identifies two new tardigrade species (Eutardigrada: Macrobiotidae) from Greenland. Eur J Taxon **614:**1–40. doi:10.5852/ejt.2020.614.

Stec D, Vecchi M, Calhim S, Michalczyk Ł. 2021a. New multilocus phylogeny reorganises the family Macrobiotidae (Eutardigrada) and unveils complex morphological evolution of the *Macrobiotus hufelandi* group. Mol Phylogenet Evol **160:**106987. doi:10.1016/j.ympev.2020.106987.

Stec D, Vecchi M, Dudziak M, Bartels PJ, Calhim S, Michalczyk Ł. 2021b. Integrative taxonomy resolves species identities within the *Macrobiotus pallarii* complex (Eutardigrada: Macrobiotidae). Zool Lett **7:**9. doi:10.1186/s40851-021-00176-w.

Stec D, Vecchi M, Maciejowski W, Michalczyk Ł. 2020c. Resolving the systematics of Richtersiidae by multilocus phylogeny and an integrative redescription of the nominal species for the genus *Crenubiotus* (Tardigrada). Sci Rep **10:**19418. doi:10.1038/s41598-020-75962-1.

Stec D, Vončina K, Kristensen RM, Michalczyk Ł. 2022. The *Macrobiotus ariekammensis* species complex provides evidence for parallel evolution of claw elongation in macrobiotid tardigrades. Zool J Linn Soc **195:**1067–1099. doi:10.1093/zoolinnean/zlab101.

Sun XL, Zhang JY, Wang N, Zhao M, Luo XG. 2020. A new species of *Diphascon* (Tardigrada: Hypsibiidae) from Northern China supported by integrated taxonomy. Zootaxa **4722:**185–194. doi:10.11646/zootaxa.4722.2.5.

Sun XZ. 2014. Relationship between species diversity and environment of tardigrada in China. PhD disseratation, Shaanxi Normal University. (in Chinese)

Tabachnick BG, Fidell LS. 2007. Using Multivariate Statistics, 5th ed., Allyn and Bacon, Boston, USA.

Vecchi M, Cesari M, Bertolani R, Jönsson KI, Rebecchi L, Guidetti R. 2016. Integrative systematic studies on tardigrades from Antarctica identify new genera and new species within Macrobiotoidea and Echiniscoidea. Invertebr Syst **30:**303–322. doi:10.1071/IS15033.

Vecchi M, Stec D, Tommi V, Ryndov S, Chartrain J, Calhim S. 2022. *Macrobiotus naginae* sp. nov., a new xerophilous tardigrade species from Rokua sand dunes (Finland). Zool Stud **61:**22. doi:10.6620/ZS.2022.61-22.

Wang Y. 2021. Study on tardigrada fauna and species diversity in Wumeng Mountain area. Master thesis, Shaanxi Normal University. (in Chinese)

Wełnicz W, Grohme MA, Kaczmarek Ł, Schill RO, Frohme M. 2011. ITS-2 and 18S rRNA data from *Macrobiotus polonicus* and *Milnesium tardigradum* (Eutardigrada, Tardigrada). J Zool Syst Evol Res **49:**34–39. doi:10.1111/j.1439-0469.2010.00595.x.

Yang T. 2015. Fauna Sinica Invertebrata. Vol. 50. Tardigrada. Science Press, Beijing, 279 pp. (in Chinese)

Zeller C. 2010. Untersuchung der Phylogenie von Tardigradenanhand der Genabschnitte 18S rDNA und Cytochrom *c* Oxidase Untereinheit 1 (COX I). Master thesis, Technische Hochschule Wildau 105 pp.

Zhang D, Gao F, Jakovlic I, Zou H, Zhang J, Li WX, Wang GT. 2020. PhyloSuite: an integrated and scalable desktop platform for streamlined molecular sequence data management and evolutionary phylogenetics studies. Mol Ecol Resour **7220:**348–355. doi:10.1111/1755-0998.13096.

Supplementary materials

Table S1. A list of species of the genus *Macrobiotus* (valid and doubtful taxa), and the species formally described from China are in bold. (download)

Table S2. Raw morphometric data underlying the description of *Macrobiotus hupingensis* sp. nov. (download)

Table S3. Uncorrected pairwise distances. (download)